International Journal of Modern Physics A
Vol. 20, Nos. 2 & 3 (2005) 280–290

World Scientific
www.worldscientific.com

2π-PHOTOPRODUCTION

ULRIKE THOMA

2. Physikalisches Institut, University of Giessen,
Heinrich-Buff-Ring 16, 35392 Giessen, Germany

2π-photoproduction is one of the promising reactions to search for new baryon resonances and to investigate the properties of resonances in general. Recent data taken by various experiments show interesting resonance structures. First preliminary partial wave analysis results of the $\gamma p \rightarrow p\pi^0\pi^0$-CB-ELSA data indicate the observation of baryon resonances not only decaying via $\Delta\pi$ but also via higher mass states like e.g. $D_{13}(1520)\pi$. Recently, data on polarisation observables became available, like e.g. the double polarisation data from MAMI, or the single polarisation data from GRAAL and CLAS.

Keywords: Photoproduction; baryon spectroscopy.

1. Introduction

Quantum chromodynamics (QCD) is believed to be the correct theory of strong interactions. Using perturbative methods we have access to QCD at high momentum transfer (perturbative QCD), and at very low energies in the realm of chiral perturbation theory. At medium energies, where the strong coupling constant is large and perturbative methods fail, our present understanding is still very limited. This is the energy regime of meson and baryon resonances, and one of the key issues is to identify the relevant degrees-of-freedom in this energy range and the effective forces between them. One necessary step towards this aim is undoubtedly a precise knowledge of the experimental spectrum of baryon resonances and of their properties. Their comparison with different models may lead to a deeper understanding of this energy regime. Quark models are in general amazingly successful in describing the spectrum of existing states. However constituent quark models usually predict many more resonances than have been observed so far. Different explanations have been suggested to explain this observation:
1) The "missing" states may not exist. As proposed e.g. by Lichtenberg[1], the nucleon resonances could have a quark-diquark structure. This reduces the number of internal degrees-of-freedom, and therefore, the number of existing states. Of course, one might also think of other hidden symmetries. At a first glance, this explanation seems to be rather exotic. QCD does not give us any reason to believe that the three quarks shouldn't play an equal role in the nucleon. In addition, there are no

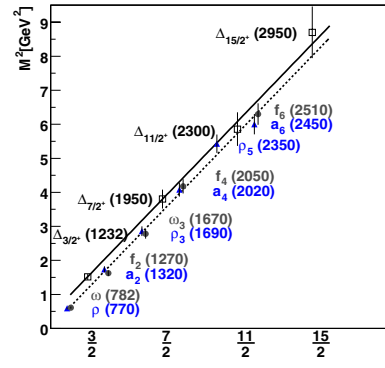

Fig. 1. Regge trajectory for Δ-resonances with even orbital angular momentum L and J=L+3/2 in comparison to the meson trajectory (J=L+S) - see Ref. 2.

hints from lattice QCD for such a quark-diquark structure. On the other hand it is interesting to notice that the Regge trajectories for mesons and baryons are parallel (Fig. 1).

The similar dependence of the mass squared on the angular momentum seems to indicate that the acting force is also very similar. This behavior could be easily understood in terms of a quark-diquark picture, with a diquark in a baryon replacing the antiquark in the meson (see also Refs. 2).

2) The "missing" states may not have been observed so far because of a lack of high quality data in channels different from πN. Most available experimental data stem from πN scattering experiments. If these states decouple from πN they would not have been observed so far. This conjecture seems reasonable following quark model predictions[3,4]. Many of these unobserved states are expected to couple significantly to channels like $\Delta\pi$ or $N\rho$ and also to γp[4,5]. Therefore photoproduction experiments investigating these channels have a great discovery potential if these resonances really exist.

Of course, the investigation of 2π-photoproduction is also interesting to determine the properties of resonances like e.g. their photo-couplings and partial widths, providing additional information which can be compared to model predictions. The properties of a resonance are also of big importance for an interpretation of its nature. One immediate debate in the light of the possible observation of a pentaquark is e.g. whether the $P_{11}(1710)$ and the $P_{11}(1440)$ might be pentaquarks rather than 3-quark-states. A good understanding of their production and decay properties may help to elucidate their nature.

2. $\gamma p \to N\pi\pi$

The magnitude of the cross section for different 2π-photoproduction channels is shown in Fig. 2. The cross section of the reaction $\gamma p \to p\pi^+\pi^-$ is clearly the largest one. It exceeds e.g. the $\gamma p \to p\pi^0\pi^0$ cross section by about one order of magnitude.

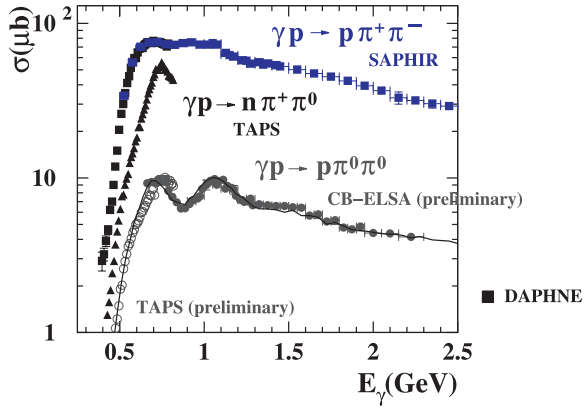

Fig. 2. 2π-photoproduction cross sections of the proton for different isospin channels. The data shown stems from different experiments, the $\gamma p \to p\pi^+\pi^-$-data from DAPHNE[6] and SAPHIR[7], the $\gamma p \to n\pi^+\pi^0$-data from TAPS[8] and the $\gamma p \to p\pi^0\pi^0$-data from TAPS[9] (empty circles at lower energies) and from CB-ELSA[10].

Within the different $\gamma p \to N2\pi$-channels the $\gamma p \to p\pi^0\pi^0$-channel is the one best suited to investigate the $\Delta\pi$ decay of baryon resonances. Compared to other isospin-channels, many non-resonant-"background" amplitudes which are important or even dominant in channels involving charged pions do not contribute. Examples are e.g. the diffractive ρ-production or the Δ-Kroll-Rudermann term. Both contribute strongly to the $\gamma p \to p\pi^+\pi^-$ channel. The latter is dominant close to threshold, where it is responsible for the strong raise of the cross section. The importance of the diffractive ρ-production increases with increasing photon energy; at higher energies it is responsible for a significant fraction of the cross section[7]. In addition, the number of possible Born terms and t-channel processes is strongly reduced in the $\gamma p \to p\pi^0\pi^0$-channel; π-exchange is e.g. not possible. This leads to a high sensitivity of the $\gamma p \to p\pi^0\pi^0$-channel to baryon resonances decaying into $\Delta\pi$. To investigate also the $N\rho$ decay of baryon resonances, channels which include charged pions need to be investigated. This decay channel is also of interest to search for new baryon resonances and to determine the properties of resonances. Since more amplitudes contribute, including the increased number of background amplitudes, the extraction of the resonant amplitudes is here much more difficult.

2.1. *The $\gamma p \to p\pi^0\pi^0$-channel – Data from TAPS and GRAAL*

The $\gamma p \to p\pi^0\pi^0$ cross section as measured by TAPS[11] in the low energy range and by GRAAL[12] up to an incoming photon energy of about 1500 MeV is shown in Fig. 3; two peak-like structures are observed.

The data has been interpreted within the Laget[13] and Valencia model[14], resulting in very different interpretations. In the Valencia-model, which is limited to the low energy region, the $D_{13}(1520)$ decaying into $\Delta(1232)\pi$ dominates the lower energy peak, while in the Laget-model the $P_{11}(1440)$ decaying into σp is clearly

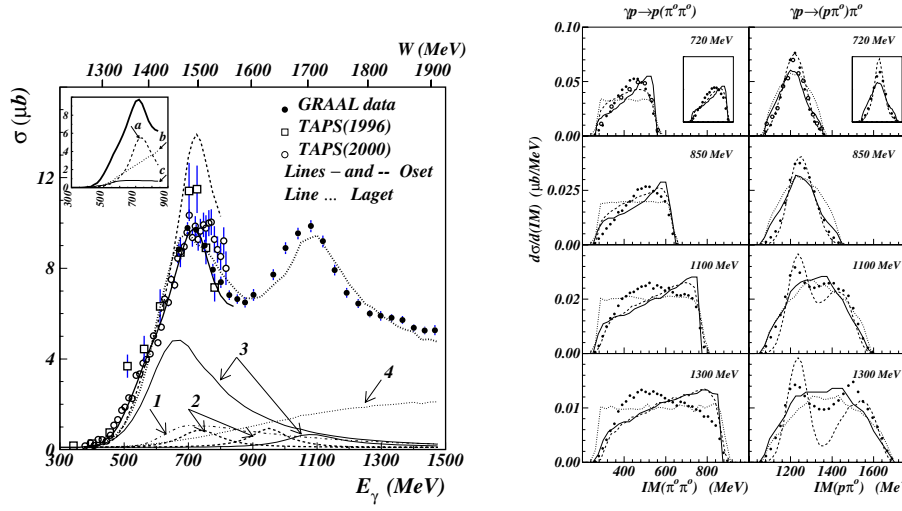

Fig. 3. $\gamma p \to p2\pi^0$-photoproduction cross sections measured by GRAAL[12] and TAPS[11], shown together with the interpretation as given by Laget[13] and within the Valencia-model[14]. Left: Total cross section, in the lower part the partial contributions as found in the Laget model are given: (1) $\gamma p \to P_{11}(1440) \to \Delta\pi$, (2) $\gamma p \to D_{13}(1520), D_{13}(1710) \to \Delta\pi$, (3) $\gamma p \to P_{11}(1440), P_{11}(1710) \to p\sigma$, (4) $\gamma p \to p\sigma$. In the inset the Valencia-model calculation is shown; lines (a), (b), (c) for $D_{13}(1520)$, Δ, and $P_{11}(1440)$ intermediate states, respectively. Right: Invariant mass spectra at four different beam energies. At E_γ=720 MeV the insets compare the Laget (solid line) and the Valencia (dashed line) model with the GRAAL data. The figures are taken from Ref. 12.

the dominant contribution. This shows that even-though both models lead to a reasonable description of the total cross section their interpretation of the data is rather different, in fact they are contradicting each other.

2.2. *The* $\gamma p \to p\pi^0\pi^0$ *data from CB-ELSA*

Recently data on $\gamma p \to p\pi^0\pi^0$ has also been taken by the CB-ELSA experiment in Bonn extending the covered photon energy range up the E_γ=3.0 GeV ($\sqrt{s}$=2.6 GeV). Due to its electromagnetic calorimeter consisting of 1380 CsI(Tl) crystals covering 98% of the 4π solid angle, the CB-ELSA detector (Fig. 4, left) is very well suited to measure photons.

To investigate the reaction $\gamma p \to p\pi^0\pi^0$, events are selected with 4 photons measured in the calorimeter and a proton identified in a 3-layer scintillating fiber detector. The reactions $\gamma p \to p\pi^0\pi^0$ and $\gamma p \to p\pi^0\eta$ are clearly observed (Fig. 4, right).

Decay Dalitz plots for different bins in $\sqrt{s}$ are shown in Fig 5. These plots indicate how possible resonances in the corresponding mass ranges might decay. The lowest $\sqrt{s}$-bin is clearly dominated by $\Delta\pi$-events. In the higher $\sqrt{s}$-bins, additional contributions become visible, like e.g. a bandlike structure in the region of 1520 MeV and 1660 MeV. The observed structures may hint at baryon resonances

decaying into $\Delta(1232)\pi$, $D_{13}(1520)\pi$, and into $X(\sim 1660)\pi$. A partial wave analysis, discussed below, confirms the existence of baryon resonances decaying via the above mentioned channels.

2.2.1. *Preliminary partial wave analysis of the $\gamma p \to p\pi^0\pi^0$ data*

To extract the contributing resonances, their quantum numbers and their properties from the data, a partial wave analysis (PWA) needs to be done. The formalism used is summarized in[15]. The fit uses Breit-Wigner resonances and includes s- and t-channel amplitudes. An unbinned maximum-likelihood fit was performed which has the big advantage of being event-based; it takes all the correlations between the five independent variables correctly into account. When only differential cross sections are fitted, the information on the correlations between the different variables is lost. The fits include the preliminary TAPS data[9] in the low energy region in addition to the CB-ELSA data. The latter was taken using two different energy settings (E_{e^-}=1.4 GeV, 3.2 GeV). Resonances with different quantum numbers were introduced in various combinations allowing, so far, for the following decay modes: $\Delta(1232)\pi$, $N(\pi\pi)_s$, $P_{11}(1440)\pi$, $D_{13}(1520)\pi$ and $X(1660)\pi$. For a good description of the data resonances like e.g. the $P_{11}(1440)$, the $D_{13}(1520)$, the $D_{13}/D_{33}(1700)$, the $P_{13}(1720)$, the $F_{15}(1680)$ as well as several additional states are needed. An example for the quality of the data description reached is shown in Fig. 6.

It also shows the result of the PWA for the lower energy data set integrated over phase space (total cross section). One preliminary result of the PWA is a dominant contribution of the $D_{13}(1520) \to \Delta\pi$ amplitude in the energy range where the first peak in the cross section occurs. Fig. 7 shows the $p\pi^0$ invariant mass and angular distributions in the $\sqrt{s}$-range from 1450 MeV to 1550 MeV.

The $\Delta(1232)$ clearly dominates the $p\pi^0$ invariant mass. The PWA attributes most of these events to the $\gamma p \to D_{13}(1520) \to \Delta\pi$ amplitude (see also Ref. 11). This interpretation gets further substantiated by looking at the angular distributions. The angular distribution for the $D_{13}(1520) \to \Delta\pi$-amplitude has a very similar

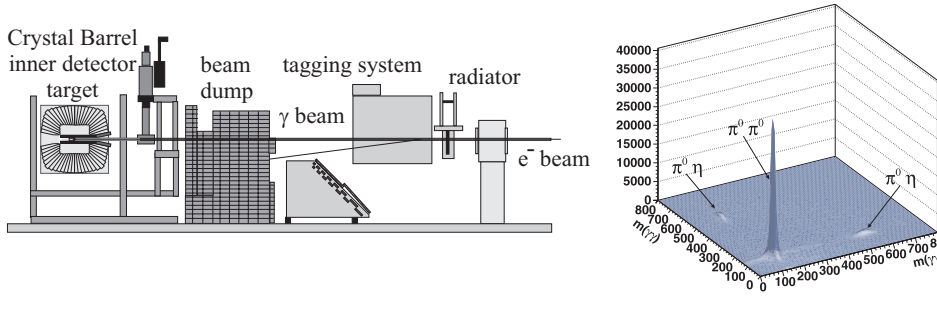

Fig. 4. Left: The Crystal Barrel detector at ELSA. Right: p4γ events: $\gamma\gamma$-invariant mass of one two-photon pair versus the $\gamma\gamma$-invariant mass of the other two-photon pair. A clear peak due to $p\pi^0\pi^0$ events and smaller enhancements due to $p\pi^0\eta$ events are observed.

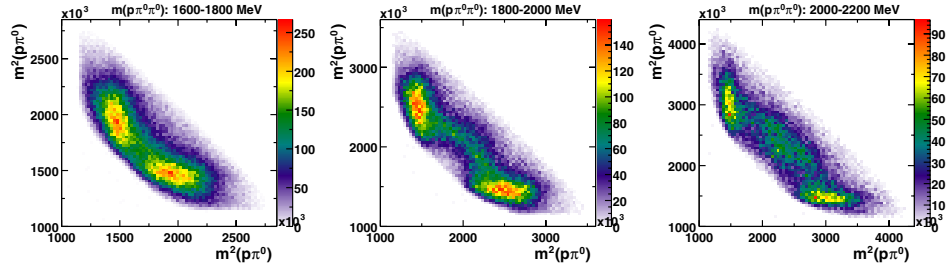

Fig. 5. Dalitz plots for different $\sqrt{s}$-bins as given above the picture. The plots are not corrected for acceptance and no flux normalization was done (preliminary).

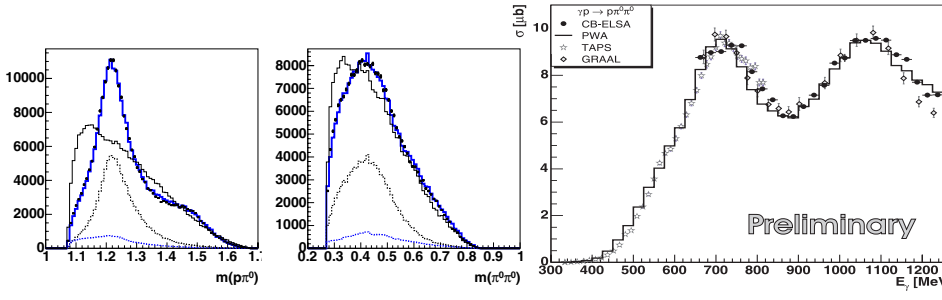

Fig. 6. Invariant mass distributions in comparison to the PWA-result for the lower energy CB-ELSA data (without acceptance correction). Each plot shows the experimental data (points with error bars), and the result of the PWA (solid gray curve). The contribution of the $D_{13}(1520)$ and the $P_{11}(1440)$ are shown as dashed black (upper) and dashed gray (lower) curves, respectively. The thin black line represents the phase space distribution. The description of the angular distributions are of similar quality. The $\gamma p \to p\pi^0\pi^0$ cross section for the lower energy data set as determined from the PWA (solid curve) in comparison to the GRAAL, TAPS, and CB-ELSA data (preliminary).

shape as the data, while the $P_{11}(1440)$ angular distribution differs significantly from the data. (The $P_{11}(1440)$ contribution includes its decay into $\Delta\pi$ and $N\sigma$ with a relative strength adjusted by the fit. The angular distributions for the separate

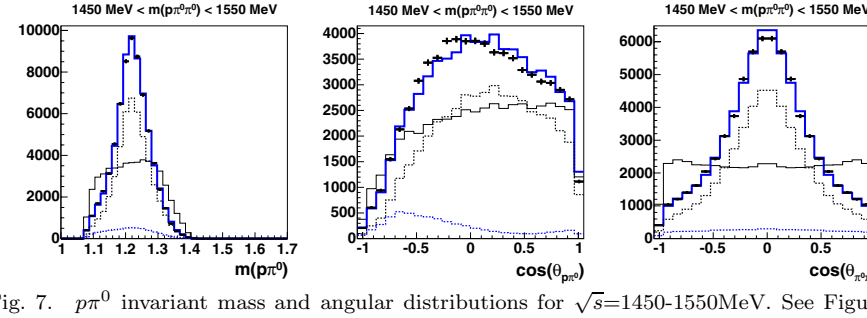

Fig. 7. $p\pi^0$ invariant mass and angular distributions for $\sqrt{s}$=1450-1550MeV. See Figure 6 for the meaning of the different curves.

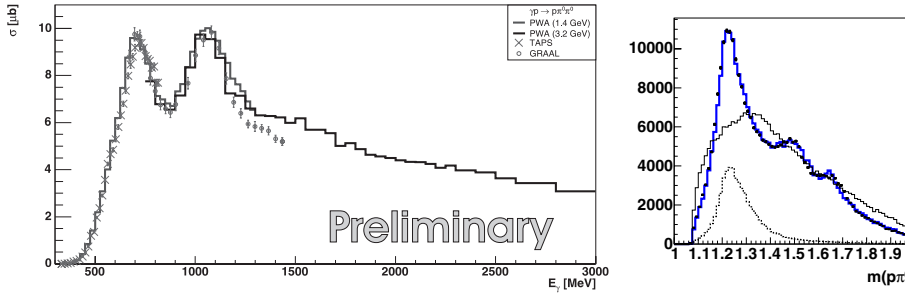

Fig. 8. Left: Total cross section as obtained by integrating the result of the partial wave analysis over phase space (solid line), in comparison to the preliminary TAPS[9] and GRAAL[12] data. Right: $p\pi^0$ invariant mass for the higher energy data set (E_γ=0.8-3.0 GeV) in comparison to the result of the PWA. See Figure 6 for the meaning of the different curves.

decay amplitudes differ strongly from the data as well). The preliminary result of our analysis is therefore in contradiction to the interpretation given within the Laget model, where the $P_{11}(1440) \rightarrow p\sigma$-amplitude dominates in this energy range.

Fig. 8 shows the total cross section obtained by fitting the two CB-ELSA data sets and the TAPS data and by integrating the result of the combined fit over phase space.

In the CB-ELSA data baryon resonances not only decaying into $\Delta\pi$ but also via $D_{13}(1520)\pi$ and $X(1660)\pi$ are observed for the first time. The enhancements at the corresponding $p\pi$ invariant masses are visible in the Dalitz plots (Fig. 5) and can also be seen in Fig. 8. The observation of baryon cascades is also interesting in respect to the search for states which might not couple to πN and γp; they still could be produced in such baryon cascades.

2.3. $\vec{\gamma}\vec{p} \rightarrow p\pi^0\pi^0$ - *data from MAMI*

In respect to the question whether the main contribution in the energy region of the first peak in the $\gamma p \rightarrow p\pi^0\pi^0$ cross section stems from the $P_{11}(1440)$ or from the $D_{13}(1520)$ also the result of the $\gamma p \rightarrow p\pi^0\pi^0$ double polarisation experiment performed by the GDH-collaboration at MAMI is very interesting[17]. It was found that the $\sigma_{3/2}$ component which cannot be due to the $P_{11}(1440)$ clearly dominates in this energy region. According to the Valencia-model[14,16] which was used to describe this data, the $D_{13}(1520)$-resonance is largely responsible for the observed dominance of the $\sigma_{3/2}$ cross section. The non-negligible $\sigma_{1/2}$ component observed is presently underestminated by the Valencia-model.

2.4. $\gamma p \rightarrow p\pi^+\pi^-$ – *Data from the SAPHIR experiment at ELSA*

The SAHPIR experiment has measured the reaction $\gamma p \rightarrow p\pi^+\pi^-$ in a photon energy range from 0.5-2.6 GeV. The corresponding total cross section based on 7.7×10^6 reconstructed events is shown in Fig. 9. While being in nice agreement

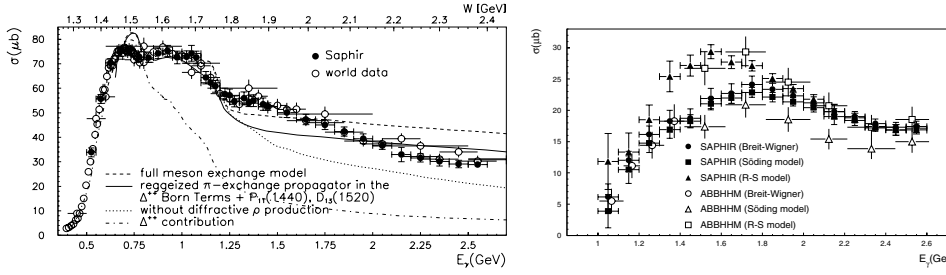

Fig. 9. Left: The total $\gamma p \to p\pi^+\pi^-$ cross section from SAPHIR[7] compared to data from Refs. 18, 19, 20, the curves are from Ref. 21. Right: Total cross sections for the reaction $\gamma p \to N\rho$ evaluated with different methods (Söding[22], Ross-Stodolsky[23]).

with the so far existing data, the new SAPHIR data substantially improves the accuracy of the existing data especially above 800 MeV.

This final state gives access to the subchannels $\gamma p \to \pi^-\Delta^{++}$, $\gamma p \to \pi^+\Delta^0$ and $\gamma p \to p\rho$. All three of them have been investigated by the SAPHIR-collaboration. For the separation of the subchannels different phenomenological models have been used. For further details see[7]. The $\gamma p \to N\rho$ cross section is shown in Fig. 9 to exemplify one of the subchannels investigated. It also shows the model dependence of the extraction of the $N\rho$-total cross section using different methods.

2.5. $\gamma p \to p\pi^+\pi^-$ – *Data from CLAS at Jefferson Laboratory*

The $\gamma p \to p\pi^+\pi^-$ channel has also been investigated by the CLAS collaboration. To analyse the data a different approach has been taken[25]. Here a set of partial waves was fitted to the data adding the t-channel amplitudes empirically. The fits have been done independently for different photon-energy bins. Integrating the results over phase space yields in the total cross section shown in Fig. 10.

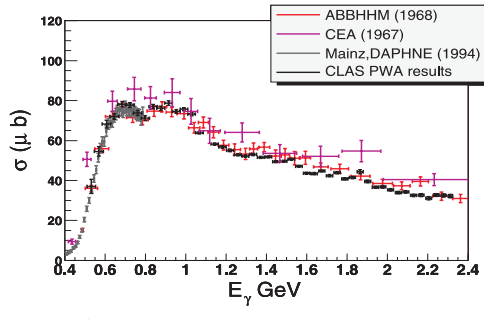

Fig. 10. Total $\gamma p \to p\pi^+\pi^-$-cross section (black points) in comparison to data from Refs. 6, 18, 24.

The preliminary cross section is in nice agreement with the data from Refs. 6, 18, 24. The analysis of this final state is still in progress but so far no evidence

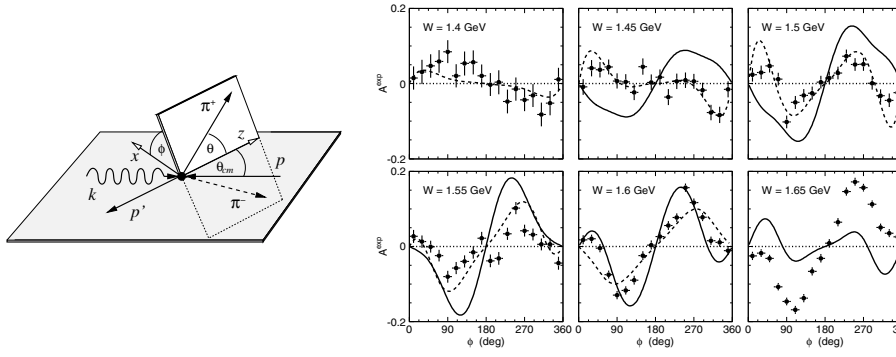

Fig. 11. Left: Angle definitions for $\vec{\gamma}p \to p\pi^+\pi^-$ in the helicity frame; θ_{cm} is defined in the overall center-of-mass frame while θ and ϕ are defined as the π^+-angles in the rest frame of the $\pi^+\pi^-$ system. Right: Measured cross section symmetry as a function of the angle ϕ plotted for different bins of $W = \sqrt{s}$. The dashed curves are calculations by Roberts (4π integrated, W$\leq$1.6 GeV), the solid curves model are calculations by Mokeev *et al.* (within CLAS acceptance, W$\geq$1.45 GeV W$\leq$1.6 GeV). The figure is taken from Ref. 28.

for new baryon resonances were found[25], even-though a combined analysis of this data together with the CLAS $p\pi^+\pi^-$ electroproduction data seems to indicate that there might be two P_{13}-resonances in the mass region around 1720 MeV[26] (see also Ref. 27).

$\vec{\gamma}p \to p\pi^+\pi^-$

CLAS has also measured the beam-helicity-dependent angular distributions for $\vec{\gamma}p \to p\pi^+\pi^-$ using a circularly-polarized tagged photon beam[28] (Fig. 11). While the total cross section (Fig. 10) does not show obvious structures, the asymmetry A strongly depends on $\sqrt{s}$ and on the angles. It is defined as follows:

$$A = \frac{1}{P_\gamma} \cdot \frac{\sigma^+ - \sigma^-}{\sigma^+ + \sigma^-}$$

where P_γ is the degree of circular polarisation and $\sigma^\pm$ is the cross section for the two photon helicity states $\lambda = \pm 1$. The angles are defined as shown in Fig. 11.

The observed asymmetry depends strongly on the kinematics of the reaction. Its comparison with the relatively structureless total cross section nicely illustrates that the measurement of polarisation variables provides additional and important constraints for partial wave analyses and models describing the data (see also Ref. 29).

3. Summary

2π-photoproduction data has been taken by various experiments showing interesting resonance structures. In the $\gamma p \to p\pi^0\pi^0$ total cross section two clear peaks around E_γ=700 MeV and 1100 MeV are observed. The interpretation of the lower energy peak has been controversially discussed. Within the Laget model the main

contribution in this energy range is due to the $P_{11}(1440) \to p\sigma$ amplitude, in the Valencia-model it is due to the $D_{13}(1520) \to \Delta\pi$. A preliminary combined partial wave analysis of the CB-ELSA and TAPS data also indicates a dominant contribution of the $D_{13}(1520)$ decaying into $\Delta\pi$ in this energy range. Preliminary double polarisation data taken by the GDH-collaboration at MAMI shows a dominant $\sigma_{3/2}$ component, which cannot be produced by a P_{11} resonance but could be explained by a dominant $D_{13}(1520)$ contribution. At higher energies, in addition to the $\Delta\pi$ decay of baryon resonances also their decay via higher mass resonances like e.g. the $D_{13}(1520)$ is observed in the CB-ELSA-data. This observation might open up a new possibility to search for baryon resonances which decouple from $N\pi$ and γN; they still might be produced baryon cascades. Recently also high quality data on $\gamma p \to p\pi^+\pi^-$ became available from SAPHIR and CLAS. This channel provides access not only to the $\Delta^{++}\pi^-$ and $\Delta^0\pi^+$ but also to the $N\rho$ channel, thus providing additional information on resonances and their decays. One important further step towards a better understanding of the data and of the resonance spectrum itself is the measurement of single and double polarisation variables. Such polarisation data has been taken recently by various experiments e.g. by GRAAL, at MAMI, by CLAS, and by CB-ELSA/TAPS. New measurements will also take place in near future, like e.g. double polarisation experiments at ELSA.

Acknowledgments

The author acknowledges an Emmy Noether grant from the Deutsche Forschungsgemeinschaft.

References

1. D.B. Lichtenberg, *Phys. Rev.* **178**, 2197 (1969).
2. E. Klempt, *Phys. Rev.* **C66**, 058201 (2002).
3. S. Capstick, W. Roberts, *Phys. Rev.* **D47**, 1994 (1993).
4. S. Capstick, W. Roberts, *Phys. Rev.* **D49**, 4570 (1994).
5. S. Capstick, *Phys. Rev.* **D46**, 2864 (1992).
6. A. Braghieri *et al.*, *Phys. Lett.* **B551**, 46 (1995).
7. C. Wu *et al.* [SAPHIR collaboration], submitted for publication to *Eur. Phys. J.*
8. W. Langärtner *et al.*, *Phys. Rev. Lett.* **87**, 052001 (2001).
9. M. Kotulla, private communication.
10. U. Thoma, M. Fuchs *et al.* [CB-ELSA collaboration], in preparation.
11. M. Wolf *et al.*, *Eur. Phys. J.* **A9**, 5 (2000);
    F. Härter *et al.*, *Phys. Lett.* **B401**, 229 (1997).
12. Y. Assafiri *et al.*, *Phys. Rev. Lett.* **90**, 222001 (2003).
13. J.-M. Laget, L.Y. Murphy, shown in Ref. 12.
14. J.A. Gomez Tejedor *et al.*, *Nucl. Phys.* **A600**, 413 (1996).
15. A. Anisovich, E. Klempt, A. Sarantsev, U. Thoma, submitted to *Eur. Phys. J.* **A**; *hep-ph/0407211*.
16. J. Nacher *et al.*, *Nucl. Phys.* **A695**, 295 (2001); *Nucl. Phys.* **A697**, 372 (2002).
17. H.-J. Arends, talk at NSTAR 2004; J. Ahrens *et al.*, in preparation.
18. ABBHHM-collaboration, *Phys. Rev.* **175**, 1669 (1968); *Phys. Rev.* **188**, 2060 (1969).

19. A. Braghieri *et al.*, *Phys. Lett.* **B363**, 46 (1995).
20. J. Ballam *et al.*, *Phys. Rev.* **D5**, 15 (1972).
21. L.Y. Murphy, J.-M. Laget, DAPHINA-SPHN-96-10 (1996).
22. D. Lüke, P. Söding, *Springer Tracts in Modern Physics* **59**, 39 (1971); P. Söding, *Phys. Rev. Lett.* **19**, 702 (1966).
23. M. Ross, L. Stodolsky, *Phys. Rev.* **149**, 1172 (1966).
24. Cambridge Bubble Chamber Group, *Phys. Rev.* **163**, 1510 (1967).
25. M. Bellis, PhD thesis, RPI (2003); M. Bellis talk at NSTAR'2004.
26. V. Mokeev, private communication; V. Mokeev, talk at QNP'2004, Bloomington, USA.
27. M. Ripani, *Phys. Rev. Lett.* **91**, 022002 (2003).
28. S. Strauch [CLAS collaboration], submitted to Proceedings of the Workshop on the Physics of Excited Nucleons, NSTAR 2004 (World Scientific); *nucl-ex/0407008.*
29. L. Roca, *nucl-th/0407049.*